ORCA – Online Research @ Cardiff

This is an Open Access document downloaded from ORCA, Cardiff University's institutional repository:https://orca.cardiff.ac.uk/id/eprint/147214/

This is the author’s version of a work that was submitted to / accepted for publication.

Citation for final published version:

Wang, Y.-C., Slater, T.J.A. , Leteba, G.M., Roseman, A.M., Race, C.P., Young, N.P., Kirkland, A.I., Lang, C.I. and Haigh, S.J. 2019. Imaging three-dimensional elemental inhomogeneity in Pt-Ni nanoparticles using spectroscopic single particle reconstruction. Nano Letters 19 (2) , pp. 732-738. 10.1021/acs.nanolett.8b03768

Publishers page: https://doi.org/10.1021/acs.nanolett.8b03768

Please note:
Changes made as a result of publishing processes such as copy-editing, formatting and page numbers may not be reflected in this version. For the definitive version of this publication, please refer to the published source. You are advised to consult the publisher’s version if you wish to cite this paper.

This version is being made available in accordance with publisher policies. See http://orca.cf.ac.uk/policies.html for usage policies. Copyright and moral rights for publications made available in ORCA are retained by the copyright holders.

This is an open access article published under a Creative Commons Attribution (CC-BY) License, which permits unrestricted use, distribution and reproduction in any medium, provided the author and source are cited.

ACS AuthorChoice

NANO LETTERS

Letter

Cite This: *Nano Lett.* 2019, 19, 732−738

pubs.acs.org/NanoLett

Downloaded via 82.4.106.56 on February 23, 2022 at 10:38:49 (UTC).
See https://pubs.acs.org/sharingguidelines for options on how to legitimately share published articles.

Imaging Three-Dimensional Elemental Inhomogeneity in Pt−Ni Nanoparticles Using Spectroscopic Single Particle Reconstruction

Yi-Chi Wang,[†] Thomas J. A. Slater,[*,†,‡] Gerard M. Leteba,[§] Alan M. Roseman,[∥] Christopher P. Race,[†] Neil P. Young,[⊥] Angus I. Kirkland,[‡,⊥] Candace I. Lang,[#] and Sarah J. Haigh[*,†]

[†]School of Materials, University of Manchester, Oxford Road, Manchester M13 9PL, United Kingdom

[‡]Electron Physical Sciences Imaging Centre, Diamond Light Source Ltd., Oxfordshire OX11 0DE, United Kingdom

[§]Catalysis Institute, Department of Chemical Engineering, University of Cape Town, Rondebosch 7701, South Africa

[∥]Division of Molecular and Cellular Function, School of Biological Sciences, Faculty of Biology, Medicine and Health, Manchester Academic Health Science Centre, University of Manchester, Manchester M13 9PL, United Kingdom

[⊥]Department of Materials, University of Oxford, Parks Road, Oxford OX1 3PH, United Kingdom

[#]School of Engineering, Macquarie University, Macquarie Park, NSW 2109 Australia

Supporting Information

ABSTRACT: The properties of nanoparticles are known to critically depend on their local chemistry but characterizing three-dimensional (3D) elemental segregation at the nanometer scale is highly challenging. Scanning transmission electron microscope (STEM) tomographic imaging is one of the few techniques able to measure local chemistry for inorganic nanoparticles but conventional methodologies often fail due to the high electron dose imparted. Here, we demonstrate realization of a new spectroscopic single particle reconstruction approach built on a method developed by structural biologists. We apply this technique to the imaging of PtNi nanocatalysts and find new evidence of a complex inhomogeneous alloying with a Pt-rich core, a Ni-rich hollow octahedral intermediate shell and a Pt-rich rhombic dodecahedral skeleton framework with less Pt at ⟨100⟩ vertices. The ability to gain evidence of local surface enrichment that varies with the crystallographic orientation of facets and vertices is expected to provide significant insight toward the development of nanoparticles for sensing, medical imaging, and catalysis.

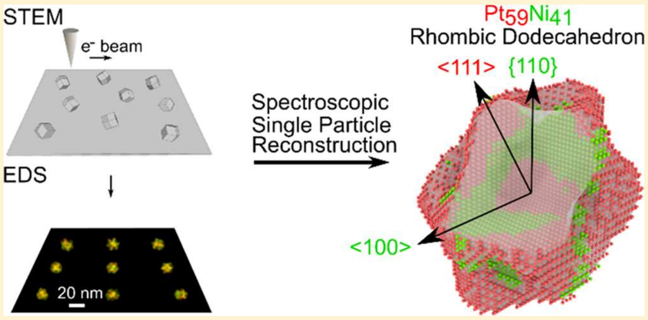

KEYWORDS: *Three-dimensional reconstruction, single particle reconstruction, PtNi nanoparticle catalysts, energy dispersive X-ray spectroscopy, surface segregation, scanning transmission electron microscopy*

Nanoparticles (NPs) are crucially important in many scientific fields, from inorganic particles[1,2] in catalysis, plasmonics, and medical imaging to proteins[3] in cellular processes. These nanoparticles may have complex morphologies and compositional disorder, both of which contribute to their properties. Electron microscopy is a valuable tool to characterize the structure and chemistry of individual NPs. However, conventional (scanning) transmission electron microscope ((S)TEM) imaging measures two-dimensional (2D) projections of 3D objects, which often prevents the interpretation of complex 3D elemental distributions because chemical information is integrated in the third dimension.

There are several established acquisition schemes for 3D characterization of individual NPs in the (S)TEM.[4−13] Tilt-series electron tomography (ET) in particular has become a common acquisition method in 3D imaging for materials science. The tilt-series ET approach is similar to X-ray computed tomography (CT); it requires multiple images of the sample viewed along different directions, which are then reconstructed to create a 3D distribution of some property of the object. Beyond characterizing 3D morphology, ET-based approaches have the ability to map elemental distributions and other physical properties, such as localized surface plasmons,[7] when STEM imaging is combined with spectroscopic techniques such as energy dispersive X-ray spectroscopy (EDS)[14−16] and electron energy loss spectroscopy (EELS).[17,18] However, tilt-series ET-based approaches require repeated imaging of the same area, which often results in a high cumulative electron dose and may cause the technique to fail for even moderately beam sensitive samples. The total fluence required, the number of electrons per square area of the sample, is dependent on the required resolution. The typical electron fluence used for high-angle annular dark-field

Received: September 17, 2018
Revised: November 11, 2018
Published: January 25, 2019

© 2019 American Chemical Society

DOI: 10.1021/acs.nanolett.8b03768
Nano Lett. 2019, 19, 732−738

(HAADF) tomography is about 10^6 electrons/Å^2 for a spatial resolution of the order of 1 nm (Supporting Information Table S1). The requirement for high electron fluence is even greater when elemental information is required with typical requirements for STEM-EDS tomography[14,15] often exceeding 10^8 electrons/Å^2 for a similar spatial resolution (Table S1). Although, for some materials electron beam damage can be reduced or eliminated by imaging with a low accelerating voltage or low electron flux, the majority of specimens are found to have a critical electron fluence above which the specimen is permanently damaged. As (S)TEM instrumentation has improved, the instability of specimens under prolonged electron irradiation is often the principal obstacle to 3D imaging.

Organic biological structures such as proteins and viruses are typically many orders of magnitude more sensitive to the electron beam than common inorganic specimens. Acquiring 3D information for such highly beam sensitive objects requires an approach termed single particle reconstruction (SPR),[19−26] which combines the information from single images of many thousands of individual objects. This technique assumes that all the objects being imaged are identical but are randomly orientated on a support. The great importance of this approach was recognized with the awarding of the Nobel prize for Chemistry in 2017,[20] but single particle reconstruction approaches have not yet been successfully applied to spectroscopic STEM data. Here, we demonstrate that by modifying the SPR approach to use STEM-EDS spectrum images rather than conventional (S)TEM data sets, we are able to recover quantitative 3D elemental information with a resolution of ~1 nm. This is achieved with an electron fluence per particle that is 500 times lower than would be required to achieve the same results using conventional STEM-EDS ET techniques (2×10^6 compared to 9×10^8 electrons/Å^2, Table S1).

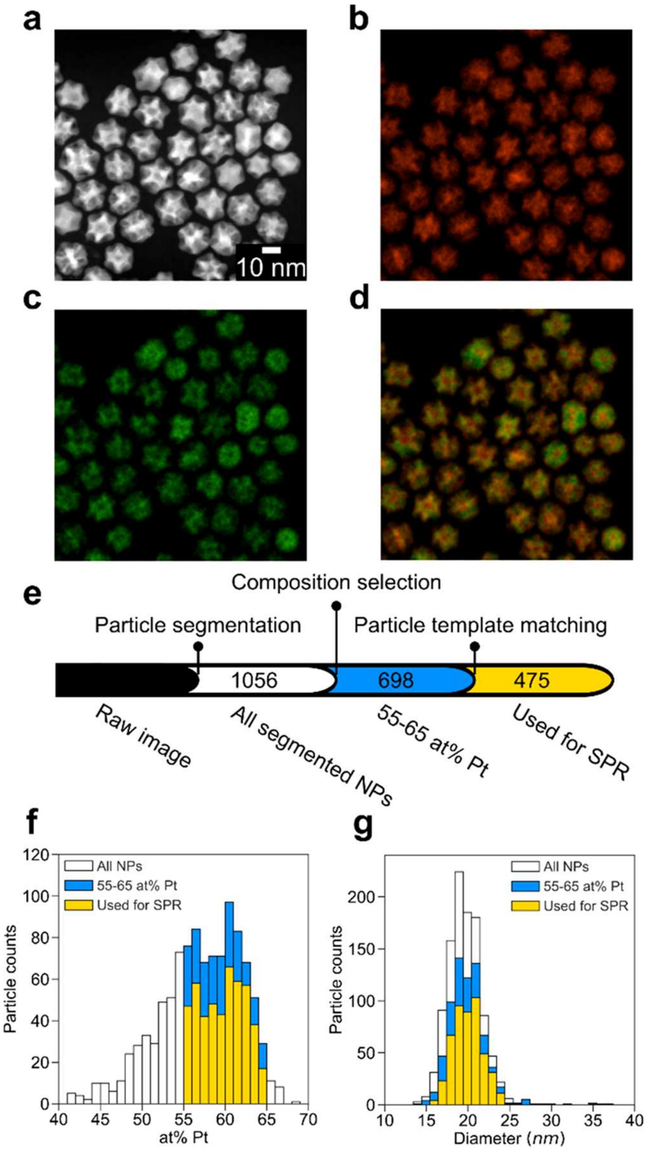

Figure 1. Overview of the PtNi NP population and quantification of specimen homogeneity. (a) Representative STEM-HAADF image of the PtNi nanoparticles together with elemental maps for (b) Pt (Lα), (c) Ni (Kα), and (d) Pt + Ni extracted from STEM-EDS spectrum images. (e) The sequence of image processing steps used to separate and identify nanoparticles to be used in the SPR reconstruction. Colors correspond to those used in histograms (f,g) and numbers correspond to the number of NPs remaining after each step. (f) Compositional distribution of the PtNi NP population calculated by k-factor EDS quantification. (g) Feret diameter distribution for the same particles. In (f,g) yellow bars represent the NPs that were matched with the ET template and used in final SPR reconstruction, blue bars include the NPs that were compositionally selected (limited to a range of 55−65 atom % Pt) but not matched to a projection, and white bars represent all segmented NPs in the raw data that were not included in the other two sets.

Application of Spectroscopic SPR to Catalytic Nanoparticles. We have applied our new approach to reconstruct the mean 3D elemental distribution for a population of bimetallic rhombic dodecahedral platinum−nickel (PtNi) NPs (Figure 1a−d) which are among the most active oxygen reduction reaction (ORR) catalysts ever designed.[1] These NPs are too electron beam sensitive for conventional tilt-series electron tomography at a resolution on the order of 1 nm, so previous (S)TEM studies of the material have been limited to 2D elemental mapping.[27−32] Platinum is one of the most effective and widely used catalytic materials with extensive applications in fuel cells, catalytic converters, and batteries.[1,2] Alloying Pt NPs with a second metal, such as Ni, has been shown to improve activity/durability for the ORR and hydrogen evolution reaction (HER)[1,2,33,34] in addition to reducing cost. Despite the importance of these materials, the mechanism for these improved properties is still not well understood, hindering attempts to maximize catalytic efficiency and in-service lifetime. Key to understanding the mechanism of PtNi NP performance is the ability to characterize elemental surface segregation and specific faceting behavior. Studies of elemental segregation in individual NPs have been largely restricted to 2D (S)TEM spectrum imaging,[27−32] due to the tendency of these NPs to alter their structure when subjected to high electron dose. We have independently measured the critical dose for electron beam damage in the PtNi nanoparticles used in this study and found that they have restructured after an electron dose of approximately 5×10^7 electrons/Å^2 (see Figure S7). This beam sensitivity precludes the use of a STEM-EDS tilt series tomography approach, which we have found requires an electron fluence on the order of 9×10^8 electrons/Å^2 to achieve an appreciable EDS signal-to-noise ratio (SNR) at 1 nm resolution (Table S1). For our spectroscopic SPR approach, we have employed a total electron dose (2×10^6 electrons/Å^2, Methods and Table

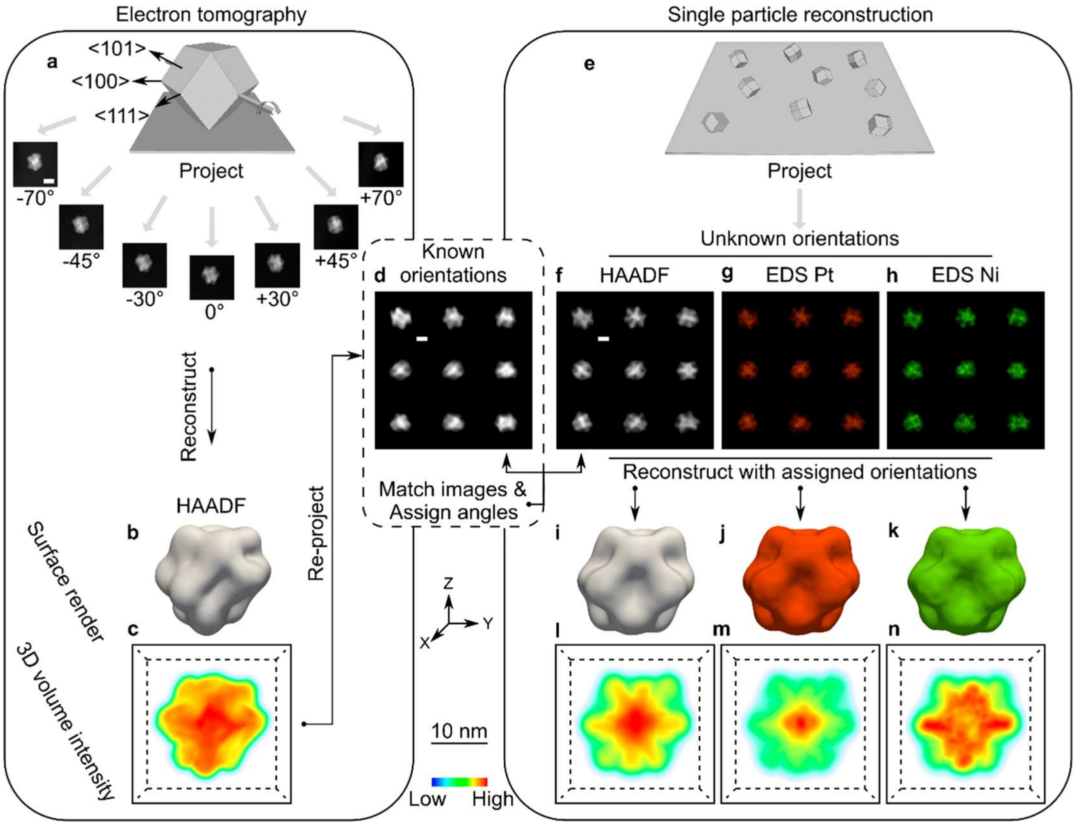

Figure 2. Workflow for spectroscopic single particle reconstruction. (a) Schematic showing the acquisition of a traditional STEM-HAADF tilt-series tomography data set for one NP. (b,c) Surface render and 3D volume intensity for the ET reconstructed HAADF signal, respectively. (d) Reprojections with known orientations obtained from the reconstruction in (b,c) (9 illustrative examples are shown from 400 reprojections). (e) Schematic of the SPR data acquisition (single images of many identical NPs with random orientations on a support film). (f) Experimental HAADF-STEM images are matched to the reprojections in panel d so as to assign known orientations. (g,h) EDS Pt and EDS Ni signals are assigned the same known orientations as have been assigned to their simultaneously acquired STEM-HAADF data in (f). (i−k) Surface renders and (l−n) 3D volume intensities for SPR reconstructed HAADF, EDS Pt, and EDS Ni 3D intensity distributions, respectively. Gray, red, and green colors in panels b,i−k represent HAADF, EDS Pt, and EDS Ni signals, respectively. In panels c,l−n, the rainbow color scaling from blue to red represents the signal intensity from minimum to maximum. Pixel values in panels g,h and reconstructed voxel values in panels j,k,m,n are EDS counts. All scale bars are 10 nm.

S1) 25 times lower than the measured critical dose for each nanoparticle (5×10^7 electrons/Å^2), which ensures that the original morphology and compositional distribution of the NPs remain the same after data acquisition (Figure S7, and Table S1).

Quantification of Nanoparticle Population Homogeneity. To perform spectroscopic single particle reconstruction, STEM-HAADF and STEM-EDS images were simultaneously acquired for over 1000 PtNi NPs as the beam is scanned pixel by pixel (an example is shown in Figure 1a−d). As the probability of generating characteristic X-rays (and of these X-rays being detected) is much lower than the probability of an electron scattering onto the HAADF detector, the SNR of the STEM-EDS elemental images is lower than the HAADF image data set. However, the direct, one-to-one correlation between the pixels in the two data sets allows the high SNR HAADF images to be used for particle identification and segmentation of both data sets (for a full description see Methods).

Inorganic nanoparticles are typically less homogeneous in size and shape than proteins and viruses, so selection criteria need to be applied to prevent outliers from deteriorating the quality of the single particle reconstruction. Analysis of the size and composition of our PtNi NPs showed unimodal distributions with a diameter of 20 ± 2 nm and composition of 56 ± 6 atom % Pt (mean ± standard deviation; Figure 1f,g, and Table S2). The majority of the NPs (698 of 1056) have a composition of 55−65 atom % Pt (blue bars in Figure 1e−g) so this subset was chosen to demonstrate our spectroscopic SPR approach. However, we note that for a bimodal or inhomogeneous nanoparticle population it is possible to perform several different reconstructions for different classes of nanoparticle, where these different classes are distinguishable in the 2D data on the basis of the particles' size, shape, or composition. To illustrate this we have separately performed an SPR reconstruction for NPs in the population with a lower Ni content (compositions of 45−55 atom % Pt, see Figures S17 and S18).

Spectroscopic Single Particle Reconstruction Workflow. The workflow we have developed for spectroscopic SPR from STEM-EDS data is illustrated in Figure 2. Initially, a conventional STEM-HAADF tilt-series ET data set is reconstructed for a single PtNi particle (Figure 2a−c, full details in Methods and Videos S1 and S2). The 3D electron tomography reconstruction serves as an initial morphological estimate that can be used to produce STEM-HAADF reprojections with known orientations (Figure 2d). The SPR input is a large data set of simultaneously acquired STEM-HAADF and STEM-EDS images in which the nanoparticle

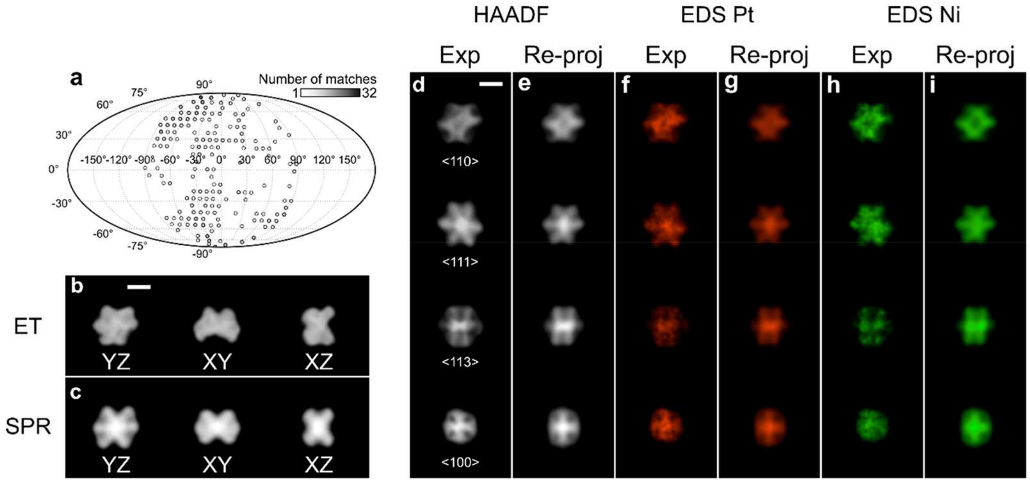

Figure 3. Verification of the fidelity of spectroscopic SPR. (a) Distribution of matched nanoparticle orientations used for SPR. (b,c) Orthoslices of *YZ*, *XY*, and *XZ* planes from ET and SPR HAADF reconstructions, respectively. The coordinate axes with respect to the 3D reconstructions are shown in Figure 2. (d,f,h) Experimental HAADF images and Pt or Ni elemental maps extracted from STEM-EDS spectrum images, respectively. (e,g,i) Reprojections generated from SPR reconstructions for HAADF STEM image, and Pt or Ni elemental maps, respectively. In (d−i), images are acquired along approximately ⟨110⟩, ⟨111⟩, ⟨113⟩, and ⟨100⟩ crystallographic directions. Scale bars are 10 nm.

orientations are unknown (Figure 2f−h, Figure S8). Orientations can be assigned to each nanoparticle in the SPR data by cross correlating the ET STEM-HAADF reprojections (Figure 2d) with the SPR STEM-HAADF experimental images (Figure 2f, Figures S11−15). Once the orientations are known, it is then possible to reconstruct 3D HAADF and EDS intensities (Figure 2i−k and Videos S3, S4, and S5).

Size analysis of the 475 SPR NP images matched to the ET reprojections showed that these particles possess the same distribution of diameters as the overall particle population, offering an initial validation of the matching process (matched particles are yellow and overall population is white in Figure 1e−g). The use of an initial HAADF tilt-series tomographic reconstruction speeds up the processing, and a similar approach has been used in conventional SPR where a low-resolution protein structure resolved by X-ray crystallography can be employed as an initial estimate for the SPR reconstruction.[3,22] Nevertheless, most inorganic nanoparticles are likely to possess a general geometric shape,[1,2,27−32] which could be used as the initial estimate for SPR,[24] particularly for nanoparticles that prove too beam sensitive for ET tilt-series acquisition.

Verification of the Fidelity of the Spectroscopic Single Particle Reconstruction. To confirm the accuracy of the orientation assignment, we perform a tilt-pair analysis for 53 NPs at 0° and 30° tilt angles (see Methods). The orientations of these tilt-pair particles were assigned using the same cross-correlation procedures applied in spectroscopic SPR. The angular differences between untilted and tilted images were calculated based on the assigned orientations, which had a mean of 29° ± 8° (mean ± standard deviation), in good agreement with the nominal goniometer tilt angle of 30° (details in Methods and Figures S9 and S10). The large standard deviation in orientation assignment is due in part to the 5° angular sampling interval used for the reprojections from the ET reconstructed template. The orientations display nearly complete angular coverage (Figure 3a), minimizing the potential for reconstruction artifacts due to the presence of a restricted tilt range in ET (commonly known as the "missing wedge" problem; Figure S6). A qualitatively good match between the perimeter shapes of orthoslices obtained from ET and SPR suggests the SPR has accurately reconstructed the morphology of the PtNi NPs (Figure 3b,c). The differences observed between the SPR and ET reconstructions are likely to be due to the SPR reconstruction being an ensemble average of hundreds of NPs, while the ET reconstruction is a single "representative" nanoparticle. In addition, comparison of experimental images and reprojections generated from the SPR reconstruction show a qualitatively good agreement for both HAADF images and elemental maps (Figure 3d−i). The high similarity of this comparison indicates that neither the NP population heterogeneity after size and composition selection or the few nonmatched orientations affect the reconstruction quality. The local reconstruction resolution, as assessed by the ResMap method,[35] is from 0.6 to 1.1 nm (see Supporting Information for a comparison of ResMap and Fourier Shell Correlation, Figures S1−4).

Visualization of 3D Chemical Inhomogeneity in the PtNi NP Populations. On the basis of the reconstructed 3D EDS intensity distribution, we performed EDS quantification to determine the elemental Pt and Ni composition for each voxel using a standardless Cliff−Lorimer approach (Figure 4) (see Supporting Information for a brief discussion of errors in the EDS quantification). Enrichment of Pt above the mean composition of 59 atom % was observed in the NP core and at vertices along ⟨111⟩ directions (red in Figure 4a,b, also indicated by the arrows in Figure 4c). Enrichment of Ni above 41 atom % occurs at the concave {110} type facets and at vertices oriented along ⟨100⟩ directions (green in Figure 4a,b, also indicated by arrows in Figure 4d). As the particles are all single crystals, we can use information from high-resolution TEM (Figure S16) or STEM images to assign the atomic structure to the reconstruction. In Figure 4a,b, spheres represent approximately four atoms to illustrate the atomic arrangement in this nanocrystal for better clarity (see Methods). A realistic atomic model was built by filling the EDS atomic percentage reconstructions with atoms in the correct crystallographic arrangement (Figure 4e,f, Figures S19 and S20 and Videos S9, S10, and S11). Individual atom species

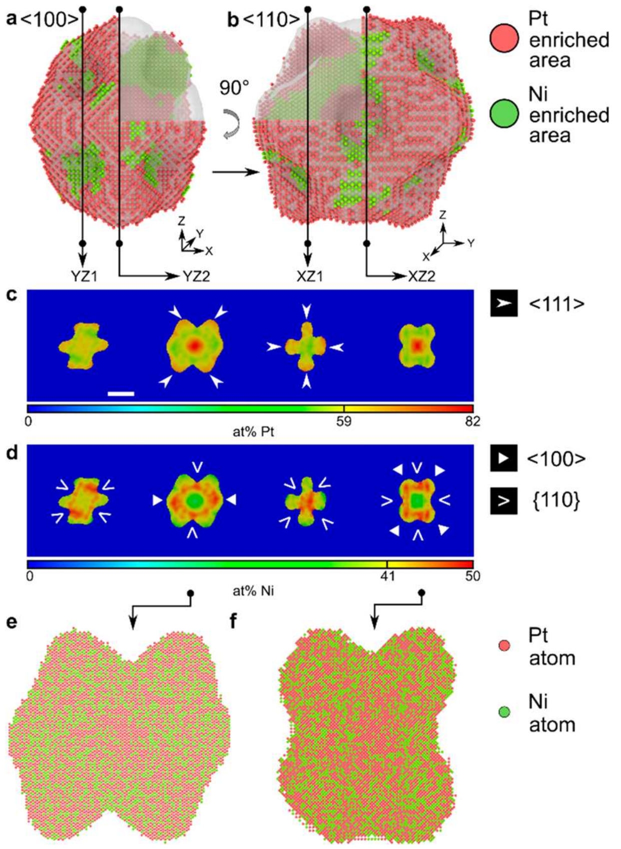

Figure 4. Visualization of 3D chemical segregation in the PtNi NP population. (a,b) Quantitative SPR elemental reconstruction thresholded at 59 atom % Pt (higher Pt content is shown red while lower Pt, above 41 atom % Ni, is shown in green) viewed along ⟨100⟩ and ⟨110⟩ directions, respectively. One eighth of the volume is cut from each reconstruction (shaded) to reveal the internal elemental distribution. Red and green balls illustrate the crystallographic arrangement of atoms in this nanocrystal. (c,d) Slices through the elemental distributions for Pt and Ni, respectively colored to reflect the atom % for each element. Elemental enrichment on the ⟨111⟩ vertices, {110} facets, and ⟨100⟩ vertices are indicated by different arrows. Scale bar is 10 nm. (e,f) Two-atom thick slices extracted from the atomic model (Video S9). Red and green atoms are Pt and Ni, respectively. Further details of the quantitative thresholding and atom fitting are described in Methods.

(Pt or Ni) were assigned randomly using the quantitative voxel composition as a probability factor (for further information see Methods). In summary, these concave rhombic dodecahedron NPs display a complex inhomogeneous alloying with a Pt-rich core, a Ni-rich hollow octahedral intermediate shell, and a Pt-rich rhombic dodecahedral skeleton framework with less Pt at ⟨100⟩ vertices (see Videos S6, S7, S8, and S9).

Previous characterization of this important catalytic nanoparticle system was limited to 2D (S)TEM analysis,[27−32] which can be difficult to interpret due to a complex structure being projected along the third dimension. The methodology we have described provides unambiguous information on elemental segregation with details on facet-dependent elemental segregation that has previously been inaccessible. The 3D elemental reconstruction of these Pt−Ni concave rhombic dodecahedral nanoparticles is consistent with previous 2D elemental mapping results[27−32] in that it reveals a Pt rich core and Pt rich edges (Figure 4). The Pt-rich core is attributed to the Pt seeds used to nucleate the particles.[30,32]

We also observe a depletion of Pt (Ni enrichment) on all {110} faces, which has also been observed in octahedral PtNi nanoparticles.[27,28,30] However, our detailed characterization has also revealed differences in composition of the different vertices (⟨111⟩ vertices are enriched in Pt while ⟨100⟩ vertices are depleted in Pt compared to the mean NP composition). Importantly, we observe the same elemental enrichment behavior in our spectroscopic SPR reconstructions for particles with a lower mean Pt content (45−55 atom % Pt, Figures S17 and S18), suggesting this is general to the whole nanoparticle population.

Discussion. The complex compositional segregation we observed cannot be simply explained by equilibrium thermodynamics and are likely to be kinetically influenced by the synthesis route, as demonstrated by the Pt-rich seed observed in the nanoparticle core. The depletion of Ni on the surfaces is also a result of the synthesis route and may be attributed to the different strength of the interaction of Pt and Ni with the oleylamine surface ligands.[29] Ni atoms are more easily oxidized than Pt, forming soluble metal complexes, which leads to faster leaching of Ni from the surfaces during aging.[29] The different enrichment behavior of the vertices can be explained by the drive to minimize both surface energy and local lattice strain. The surface free energies[36] for Ni are 2.011 J m^{-2} for {111}, 2.368 J m^{-2} for {110}, and 2.426 J m^{-2} for {100} surface facets, whereas those for Pt are 2.299 J m^{-2} for {111}, 2.819 J m^{-2} for {110}, and 2.734 J m^{-2} for {100}. Both elements therefore strongly prefer to sit on {111} facets but Pt has the larger lattice parameter[37] (0.39 nm vs 0.35 nm for Ni) so the enrichment of Pt we observe for the {111} vertices is likely favored to minimize strain.

The distribution of Pt at different vertices will have an effect on the catalytic performance of nanoparticles. Studies of flat surfaces at different crystallographic orientations have revealed that certain orientations are strongly favored for oxygen reduction activity,[33] and we would expect certain vertices to similarly display a higher activity toward catalyzing reactions. However, the atomic arrangement and local lattice strain environments found at vertices are more complex than flat surfaces. Understanding the nature of individual surface sites at each vertex as a function of chemistry would be an interesting area for further work. Such investigations could be coupled with density functional theory or molecular dynamics calculations to study the effect of variations in vertex chemistry on catalytic properties.

We aim to develop our spectroscopic single particle reconstruction further in a number of directions. The first suggested development is with regards to the analysis of inhomogeneous nanoparticle populations. In this study, we have investigated nanoparticles with a very narrow distribution in size, morphology, and chemistry, which is a prerequisite of the reconstruction. The vast majority of inorganic nanoparticles have much wider distributions of these properties and a single particle reconstruction might not at first seem applicable. However, we have demonstrated a very simple method of prefiltering particles by size and composition that we have shown can be used to separate the particle population in to different "classes" that can each be reconstructed separately. We suggest that application of more complex prefiltering, for example, by using machine learning approaches, could allow sorting of nanoparticles in to tens or hundreds of "classes", each providing a unique reconstruction, which could then be ranked by statistical significance in terms of the overall population. This is one clear advantage of the single particle reconstruction technique when compared to tilt-series electron tomography; the reconstruction obtained is representative of a larger subset of the nanoparticle population. The corresponding drawback is that features possessed by only a few particles may be lost in the reconstruction. One clear future direction for this research will be to optimize particle selection to balance the number of classes and the number of identical particles in each class to perform a reconstruction with a high signal-to-noise ratio that is representative of a significant part of the nanoparticle population.

Additionally, utilizing the structural symmetry of the nanoparticle could increase the SNR further but may generate artifacts, since the imposed symmetry must be fulfilled during orientation matching and reconstruction. For example, the highest order symmetry applicable to the nanoparticles investigated here is octahedral, which should result in a 12-fold increase in SNR. We plan to utilize higher order symmetries in future reconstructions but demonstrate here that this is not necessary to achieve an appreciable SNR and therefore nanoparticles possessing no symmetry could be faithfully reconstructed.

The SPR approach we developed can also be extended to other spectroscopic signals available in the microscope. For example, EELS could be used to map elemental distributions, bulk plasmons, or oxidation states of geometric nanoparticles using the technique. In particular, the higher signal collection efficiency of EELS may give it an advantage in 3D mapping of lower atomic number elements.

In conclusion, we have developed a novel methodology for spectroscopic STEM-EDS single particle reconstruction for characterization of 3D elemental distribution at the nanometer scale. Here we have applied the approach to relatively large NPs (~20 nm in diameter) but it would be an interesting next step to push the reconstruction resolution of the approach to resolve atomic chemistry for smaller particles. It could then be compared to another STEM-based 3D reconstruction technique of atom counting,[10−13] which is a powerful approach for atomic reconstruction of small particles but is currently limited to one or two component systems. Compared to traditional tilt-series STEM-EDS tomography, our SPR approach has demonstrated a near 500 times reduction in the required electron fluence per particle for the same cumulative dose in the final reconstruction and has the potential for further reduction simply by including more particle images, or through combination with sparse sampling and new reconstruction algorithms.[38−41] Our proof-of-principle study demonstrates the capabilities of the spectroscopic SPR technique to reveal complex elemental distributions within PtNi concave rhombic dodecahedral-shaped nanoparticles, which have been identified as one of the most active ORR catalysts ever designed.[1,29] The reconstruction also provides new evidence for the importance of considering the effects of crystallographic vertices and surface facets on local elemental distribution.

The importance of advanced structural and elemental characterization is being increasingly recognized as a necessary step to designing new nanomaterials with improved properties. The detailed structural information accessible using this approach is therefore likely to reduce the computational requirements for theoretical modeling of the energetics of large (>2 nm) alloy nanoparticles[42] and hence assist the realization of optimal nanoalloy NP design for catalysis, medical imaging, and sensing.

■ ASSOCIATED CONTENT

Ⓢ Supporting Information

The Supporting Information is available free of charge on the ACS Publications website at DOI: 10.1021/acs.nanolett.8b03768.

Detailed methods, discussion of spectroscopic single particle reconstruction resolution and EDS quantification errors, Figures S1−S20, Tables S1 and S2, description of videos S1−11, references (PDF)

Video S1: Tilt-series tomographic acquisition of HAADF images (AVI)

Video S2: Tilt-series tomography reconstruction of HAADF intensity (AVI)

Video S3: SPR reconstruction of HAADF intensity (AVI)

Video S4: SPR reconstruction of EDS Pt intensity (AVI)

Video S5: SPR reconstruction of EDS Ni intensity (AVI)

Video S6: 3D atomic percentage distribution of Pt (AVI)

Video S7:3D atomic percentage distribution of Ni (AVI)

Video S8: Composite 3D atomic percentage distribution of Pt and Ni with one-eighth cut out and thresholded at 59 atom % Pt and 41 atom % Ni (AVI)

Video S9: 3D atomic models of PtNi based on Pt and Ni 3D atomic percentage distribution. The model contains 123086 Pt atoms (red) and 81040 Ni atoms (green) (AVI)

Video S10: Two atom thick slices through the atomic models presented in Video S9. Viewed from the ⟨110⟩ direction (AVI)

Video S11: Two atom thick slices through the atomic models presented in Video S9. Viewed from the ⟨100⟩ direction (AVI)

■ AUTHOR INFORMATION

Corresponding Authors

*E-mail: Sarah.haigh@manchester.ac.uk.
*E-mail: Thomas.slater@diamond.ac.uk.

ORCID

Gerard M. Leteba: 0000-0001-7982-5037
Sarah J. Haigh: 0000-0001-5509-6706

Author Contributions

S.J.H. and T.J.A.S. conceived the idea and supervised the project. T.J.A.S. and Y.-C.W. acquired data. Y.-C.W. processed, interpreted and visualized data. G.L. and C.L. synthesized nanoparticles. Y.-C.W., T.J.A.S. and S.J.H. wrote the manuscript. A.M.R. helped with the improvement of the reconstruction quality. C.P.R. built a preliminary atomic model. N.P.Y. and A.I.K. performed preliminary TEM characterization. All authors commented on the manuscript.

Notes

The authors declare no competing financial interest.

■ ACKNOWLEDGMENTS

S.J.H., T.J.A.S., and Y.-C.W., acknowledge funding from the European Research Council (ERC) under the European Union's Horizon 2020 research and innovation programme (through the Hetero2D Synergy Grant and Grant Agreement ERC-2016-STG-EvoluTEM-715502), from the Engineering and Physical Sciences research council (EPSRC) U.K grants EP/G035954/1, EP/K016946/1, EP/J021172/1 and EP/P009050/1, the NowNANO CDT, and the Defense Threat Reduction Agency Grant HDTRA1-12-1-0013. Y.-C.W. acknowledges funding from the China Scholarship Council (CSC).

■ REFERENCES

(1) Strasser, P.; Gliech, M.; Kuehl, S.; Moeller, T. *Chem. Soc. Rev.* **2018**, *47*, 715−735.

(2) Gilroy, K. D.; Ruditskiy, A.; Peng, H. C.; Qin, D.; Xia, Y. *Chem. Rev.* **2016**, *116*, 10414−10472.

(3) Fernandez-Leiro, R.; Scheres, S. H. W. *Nature* **2016**, *537*, 339−346.

(4) Midgley, P. A.; Dunin-Borkowski, R. E. *Nat. Mater.* **2009**, *8*, 271−280.

(5) Scott, M. C.; Chen, C.-C.; Mecklenburg, M.; Zhu, C.; Xu, R.; Ercius, P.; Dahmen, U.; Regan, B. C.; Miao, J. *Nature* **2012**, *483*, 444−447.

(6) Goris, B.; Bals, S.; Van den Broek, W.; Carbó-Argibay, E.; Gómez-Graña, S.; Liz-Marzán, L. M.; Van Tendeloo, G. *Nat. Mater.* **2012**, *11*, 930−935.

(7) Nicoletti, O.; de la Peña, F.; Leary, R. K.; Holland, D. J.; Ducati, C.; Midgley, P. a. *Nature* **2013**, *502*, 80−84.

(8) Yang, Y.; Chen, C.-C.; Scott, M. C.; Ophus, C.; Xu, R.; Pryor, A.; Wu, L.; Sun, F.; Theis, W.; Zhou, J.; et al. *Nature* **2017**, *542*, 75.

(9) Van Dyck, D.; Jinschek, J. R.; Chen, F.-R. *Nature* **2012**, *486*, 243−246.

(10) Van Aert, S.; Batenburg, K. J.; Rossell, M. D.; Erni, R.; Van Tendeloo, G. *Nature* **2011**, *470*, 374−377.

(11) Jia, C. L.; Mi, S. B.; Barthel, J.; Wang, D. W.; Dunin-Borkowski, R. E.; Urban, K. W.; Thust, A. *Nat. Mater.* **2014**, *13*, 1044−1049.

(12) Jones, L.; Macarthur, K. E.; Fauske, V. T.; Van Helvoort, A. T. J.; Nellist, P. D. *Nano Lett.* **2014**, *14*, 6336−6341.

(13) van den Bos, K. H. W.; De Backer, A.; Martinez, G. T.; Winckelmans, N.; Bals, S.; Nellist, P. D.; Van Aert, S. *Phys. Rev. Lett.* **2016**, *116*, 246101.

(14) Slater, T. J. A.; Macedo, A.; Schroeder, S. L. M.; Burke, M. G.; O'Brien, P.; Camargo, P. H. C.; Haigh, S. J. *Nano Lett.* **2014**, *14*, 1921−1926.

(15) Slater, T. J. A.; Janssen, A.; Camargo, P. H. C.; Burke, M. G.; Zaluzec, N. J.; Haigh, S. J. *Ultramicroscopy* **2016**, *162*, 61−73.

(16) Rueda-Fonseca, P.; Robin, E.; Bellet-Amalric, E.; Lopez-Haro, M.; Den Hertog, M.; Genuist, Y.; André, R.; Artioli, A.; Tatarenko, S.; Ferrand, D.; et al. *Nano Lett.* **2016**, *16*, 1637−1642.

(17) Jarausch, K.; Thomas, P.; Leonard, D. N.; Twesten, R.; Booth, C. R. *Ultramicroscopy* **2009**, *109*, 326−337.

(18) Haberfehlner, G.; Orthacker, A.; Albu, M.; Li, J.; Kothleitner, G. *Nanoscale* **2014**, *6*, 14563−14569.

(19) Frank, J. *Nat. Protoc.* **2017**, *12*, 209−212.

(20) Nobelprize.org. *The Nobel Prize in Chemistry 2017*. http://www.nobelprize.org/nobel_prizes/chemistry/laureates/2017/ (accessed Apr 10, 2018).

(21) Henderson, R. *Arch. Biochem. Biophys.* **2015**, *581*, 19.

(22) Cheng, Y.; Grigorieff, N.; Penczek, P. A.; Walz, T. *Cell* **2015**, *161*, 438−449.

(23) Rosenthal, P. B.; Henderson, R. J. *J. Mol. Biol.* **2003**, *333*, 721−745.

(24) Tang, G.; Peng, L.; Baldwin, P. R.; Mann, D. S.; Jiang, W.; Rees, I.; Ludtke, S. J. *J. Struct. Biol.* **2007**, *157*, 38−46.

(25) Baldwin, P. R.; Penczek, P. A. *J. Struct. Biol.* **2007**, *157*, 250−261.

(26) Pan, Y.-H.; Sader, K.; Powell, J. J.; Bleloch, A.; Gass, M.; Trinick, J.; Warley, A.; Li, A.; Brydson, R.; Brown, A. *J. Struct. Biol.* **2009**, *166*, 22−31.

(27) Cui, C.; Gan, L.; Heggen, M.; Rudi, S.; Strasser, P. *Nat. Mater.* **2013**, *12*, 765−771.

(28) Gan, L.; Cui, C.; Heggen, M.; Dionigi, F.; Rudi, S.; Strasser, P. *Science* **2014**, *346*, 1502−1506.

(29) Chen, C.; Kang, Y.; Huo, Z.; Zhu, Z.; Huang, W.; Xin, H. L.; Snyder, J. D.; Li, D.; Herron, J. A.; Mavrikakis, M.; et al. *Science* **2014**, *343*, 1339−1343.

(30) Oh, A.; Baik, H.; Choi, D. S.; Cheon, J. Y.; Kim, B.; Kim, H.; Kwon, S. J.; Joo, S. H.; Jung, Y.; Lee, K. *ACS Nano* **2015**, *9*, 2856−2867.

(31) Niu, Z.; Becknell, N.; Yu, Y.; Kim, D.; Chen, C.; Kornienko, N.; Somorjai, G. A.; Yang, P. *Nat. Mater.* **2016**, *15*, 1188−1194.

(32) Chang, Q.; Xu, Y.; Duan, Z.; Xiao, F.; Fu, F.; Hong, Y.; Kim, J.; Choi, S.-I. Il; Su, D.; Shao, M. *Nano Lett.* **2017**, *17*, 3926−3931.

(33) Stamenkovic, V. R.; Fowler, B.; Mun, B. S.; Wang, G.; Ross, P. N.; Lucas, C. A.; Marković, N. M. *Science* **2007**, *315*, 493−497.

(34) Stamenkovic, V. R.; Mun, B. S.; Arenz, M.; Mayrhofer, K. J. J.; Lucas, C. a.; Wang, G. F.; Ross, P. N.; Markovic, N. M. *Nat. Mater.* **2007**, *6*, 241−247.

(35) Kucukelbir, A.; Sigworth, F. J.; Tagare, H. D. *Nat. Methods* **2014**, *11*, 63−65.

(36) Vitos, L.; Ruban, A. V.; Skriver, H. L.; Kollár, J. *Surf. Sci.* **1998**, *411*, 186−202.

(37) Davey, W. P. *Phys. Rev.* **1925**, *25*, 753−761.

(38) Saghi, Z.; Holland, D. J.; Leary, R.; Falqui, A.; Bertoni, G.; Sederman, A. J.; Gladden, L. F.; Midgley, P. a. *Nano Lett.* **2011**, *11*, 4666−4673.

(39) Goris, B.; Van den Broek, W.; Batenburg, K. J.; Heidari Mezerji, H.; Bals, S. *Ultramicroscopy* **2012**, *113*, 120−130.

(40) Leary, R.; Saghi, Z.; Midgley, P. A.; Holland, D. J. *Ultramicroscopy* **2013**, *131*, 70−91.

(41) Saghi, Z.; Benning, M.; Leary, R.; Macias-Montero, M.; Borras, A.; Midgley, P. a. *Adv. Struct. Chem. Imaging* **2015**, *1*, 1−10.

(42) Yan, Z.; Taylor, M. G.; Mascareno, A.; Mpourmpakis, G.; Yan, Z.; Taylor, M. G.; Mascareno, A.; Mpourmpakis, G. *Nano Lett.* **2018**, *18*, 2696.